Solar Energy Advances 1 (2021) 100008

Contents lists available at ScienceDirect

Solar Energy Advances

journal homepage: www.elsevier.com/locate/seja

The effect of wave response motion on the insolation on offshore photovoltaic installations

Ryan Bugeja [a,*], Luciano Mule' Stagno [a,b], Nicolas Branche [c]

[a] Researcher at the Institute for Sustainable Energy, University of Malta, Barrakki Street, Marsaxlokk, Malta
[b] Director at the Institute for Sustainable Energy, University of Malta, Barrakki Street, Marsaxlokk, Malta
[c] Intern at the Institute for Sustainable Energy, Barrakki Street, Marsaxlokk, Malta

ARTICLE INFO

Keywords:
Offshore energy
Renewable energy
Solar
Photovoltaics
Insolation
Wave response

ABSTRACT

Offshore photovoltaic energy is possibly the most important future step in the harnessing of solar energy. Since no long-term offshore photovoltaic installation exists to date, various unknowns are still present, creating a research gap. For instance, floating structures will have some type of response to incoming waves. This response is highly dependent on the design of the floating structure. This response will have some effect on the insolation on offshore photovoltaic systems installed on floating structures. This research presents a simulation tool that would allow an offshore system designer to assess this effect in order to minimize it and thus, optimize the energy yield of the system. Furthermore, this simulation tool was verified with an experimental setup simulating sinusoidal wave responses and the results are presented in this research. Finally, a parametric analysis was performed taking days close to the 21st of each month of the year for photovoltaic installations facing south with fixed inclinations of 30 ° and 5 ° This research will improve the design of offshore floating platforms used for photovoltaic installations.

1. Introduction

Energy demands are predicted to increase globally by 33% between 2010 and 2030 [1]. Photovoltaic (PV) technology has become very popular nowadays and is recognized as one of the most reliable sources of renewable energy. The majority of the world is striving to increase its renewable energy output with the European Union, among others, setting a 2020 target of 20% renewable energy use.

In various areas around the world, land is limited and very expensive. Land pricing has a big impact when considering large renewable energy installations since this will prolong the payback period. Today, PV modules using crystalline silicon technology occupy about 6 m^2 of land per Kilowatt Peak (kWp). Amorphous silicon modules require twice as much area [2]. Thus, a one MWp solar farm will require more than 6000 m^2 of land.

Furthermore, several countries like Malta are limited both geographically and economically in renewable energy options such as onshore wind, geothermal or hydroelectric. Until today, photovoltaic installations in small islands are mostly limited to rooftops. However, not all rooftops are suitable for PV installations due to their orientation and shading from adjacent buildings. Furthermore, rooftops are also used for other services, thus reducing the available space for PV installations. Hence, these countries require other alternatives to keep increasing their renewable energy share and manage to reduce their dependency on non-renewable energy sources. Therefore, the logical way forward is to explore and study the feasibility of offshore photovoltaic farms. Offshore photovoltaics offer the potential, for small countries like Malta or other densely populated large coastal areas, to launch large solar farms that would otherwise not be possible on the limited available land. An MCST funded project, SolAqua – R&I-2012–041, has established the viability of offshore platforms and outlined the parameters under which they would be feasible [3]. Floating solar technology is gaining popularity, especially in countries which have land space limitations [4]. Recently, China has installed 40 MWp and 70 MWp floating photovoltaic plants [5] and are approaching completion of a 150 MWp project. Furthermore, an Indonesian power company is planning a 200 MWp floating photovoltaic farm [6].

Floating PV installations have numerous advantages over land-based installations. Previous studies have shown that efficiency and yield improve due to the cooling effect of water and also the reduction in dust effects [7,4,8]. Moreover, on fresh water bodies, a floating installation can be beneficial to the surrounding environment by reducing water evaporation and improving water quality by inhibiting algal growth [9]. However, floating installations present various challenges especially when it comes to the structure design and anchoring [4]. Other issues such as high moisture levels, the durability and survivability of the installation also need to be kept in mind when designing and installing floating photovoltaics [8]. Most of the floating photovoltaic installations so far were

* Corresponding author.
E-mail addresses: ryan.m.bugeja@um.edu.mt (R. Bugeja), luciano.mule-stagno@um.edu.mt (L. Mule' Stagno), nicolas-branche@hotmail.fr (N. Branche).

https://doi.org/10.1016/j.seja.2021.100008
Received 1 February 2021; Received in revised form 30 August 2021; Accepted 17 October 2021
Available online 28 October 2021

Nomenclature

PV	photovoltaic
RES	renewable energy share
kW_p	kilowatt peak
α_s	solar altitude angle
γ_s	solar azimuth angle
LST	local standard Time
AST	apparent solar time
$B(\beta,\gamma)$	beam radiation on tilted surface
$D(\beta,\gamma)$	diffused radiation on tilted surface
$D_g(\beta, \gamma)$	diffused radiation from ground
γ	azimuth of tilted surface
A	active area of photovoltaic module
T_c	solar cell temperature (°C)
r	distance between sun and earth (km)
ε_o	eccentricity correction factor
δ	solar declination angle
F_1, F_2	circumsolar and horizon brightness coefficients
NOAA	national oceanic and atmospheric administration
ε	perez clearness coefficient
Δ	perez brightness coefficient
G_{PV}	solar radiation incident on the photovoltaic module (W/m^2)
ω	hour angle
θ_z	zenith angle
θ	beam radiation angle
$\emptyset$	latitude of tilted surface
$D_a(\beta, \gamma)$	Isotropic Sky diffused radiation
P_{MPP}	maximum power point (W)
n_{Tref}	photoelectric conversion efficiency at reference temperature
β_0	temperature coefficient
T_a	ambient temperature (°C)
r_o	deviation of Earth's orbit from the circular (km)
E	equation of time
R_{T-H}	ratio between beam radiation on tilted surface and horizontal beam radiation
FPV	floating photovoltaic

designed and installed on lakes, dams or reservoirs. Environmental and climatic issues in these areas are not as severe as those found in marine environments [7] making the design of such systems less critical. Offshore installations need to cater for constant exposure to corrosion effects of salt and the mechanical forces from a combination of wind, waves and tides [10]. Furthermore, the motion of the offshore floating structure in response to incoming waves can have an effect on the insolation on photovoltaic modules with limited research quantifying this effect.

The aim of this study is to investigate the effect of wave response motion on the insolation on offshore photovoltaic installations.

2. Literature review

The maximum power, P_{MPP} (W), delivered by a photovoltaic module at a particular time interval is highly dependent on the solar radiation incident on the module, G_{PV} (W/m^2), the solar cell temperature, T_c (°C), the photoelectric conversion efficiency of the solar cell, n_{Tref}, and the active surface area of the photovoltaic module, A (m^2). Moreover, the solar cell temperature is dependent on the amount of solar radiation incident on the solar cells, the cells' efficiency and the ambient conditions such as wind and temperature, T_a (°C). Hence, the maximum power output is calculated using Eq. (1) [11] where T_{ref} is a reference temperature (usually 25 °C) and β_0 is the temperature coefficient describing the effect of temperature on the efficiency of solar cells.

$$P_{MPP} = n_{Tref}\ A\ G_{PV}\ (1 - \beta_0(T_c - T_{ref}) \quad (1)$$

Photovoltaic modules should be installed in such a way as to maximize power output. Two of the factors affecting the insolation on photovoltaics are the module's tilt and orientation. A photovoltaic module produces maximum power when placed perpendicular to incident sun rays such that the power density on the absorbing surface is equal to that of the sun. In order to find the optimal tilt angle for a PV installation, the position of the sun with respect to a point on earth must be calculated.

The location of the sun relative to a point on earth is specified mainly using the solar altitude angle (α_s) and the solar azimuth angle (γ_s). The solar altitude angle is the angle between the horizon and the position of the sun [12]. The solar azimuth angle is the angle on a plane parallel to the earth's surface measuring the sun's position from true geographic south. Therefore, optimum tilt angles for photovoltaic modules are highly dependent on the location of the installation. To calculate the optimum angle for photovoltaic installations yearly solar radiation data for that particular location is required [13]. Generally, a surface with an inclination of 10° to 15° less than the latitude, receives maximum insolation in summer while in winter an inclination of 10° to 15° more than the latitude is required for maximum insolation [13]. Mondol et al. [13] studied the impact of array inclination and orientation on a PV system installed in Northern Ireland under maritime climates and through a TRYNSYS simulation showed the variation of total annual insolation with different azimuth and tilt angles. This study concluded that a surface oriented towards south and with a tilt angle of 30°, gets maximum annual insolation. This study also showed that tilt has a much higher effect than orientation on the insolation received by a surface. A horizontal surface and a vertical south facing surface receive 9.05 and 28.7% less insolation, respectively, than a 30° south facing surface. Furthermore, for a 30° tilted surface, a change in orientation of 30° from the south results in an annual reduction of 2% surface insolation [13].

In a study based in Malta by Rebé et al. [14], it was found that although a 30° tilt results in the maximum annual power generation, this might not always be the most economical setup. When having a larger space and a multi-row PV setup, a 15° tilt design angle can house a larger number of panels due to lower separation between rows and thus result in more photovoltaic panels per unit area and an improved rate of return. Another study in Hannover, Germany [15] found that tilt angle has little effect on PV power output. However, in these studies a loss of 6% in summer and 10% in winter was still observed for non-optimal angles. A mathematical model [16] taking into consideration the variation of global irradiance, shows that an increase in power output is possible by varying a module's tilt angle between cold and hot seasons in order to compensate for the seasonal variation of the sun's position with respect to Earth. These improvements range from 3.5 to 26%, depending on the level of hourly power uniformity required. Rao and Padmanabhan [17] performed an experimental tilt angle study directly on a bare silicon solar cell under direct illumination from a laboratory light source. Therefore, this study eliminated the effects of anti-reflection coatings and glass covers in order to observe directly the behavior of a *p-n* junction at different tilt angles. This research showed that an inclination of 60 ° results in a 60% drop in power when compared to a horizontally placed solar cell, perpendicular to illumination. As discussed above, the theoretical response of a silicon solar cell to tilt variations is calculated from basic geometry due to the fact that, in a lab scenario, an inclined surface receives less insolation than a horizontal one. However, Rao and Padmanabhan showed that the experimental results differ from theory. A big part of this deviation was due to reflection losses possibly caused by the cell's surface texture. However, these reflection losses were not quantified in this study. Another factor contributing to the deviation from theory to practice is the apparent increase in junction depth. Furthermore, both the transmittance and absorptivity are dependent on incident angle. The relationship of solar transmittance to the incident

Table 1
Solar transmittance for etched and Un-etched glass as a function of incidence angle [12].

	Transmittance by Incidence Angle						
Type of Glass	0 °	20 °	40 °	50 °	60 °	70 °	80 °
Etched	0.941	0.947	0.945	0.938	0.916	0.808	0.562
Un-etched	0.888	0.894	0.903	0.886	0.854	0.736	0.468

angle is also dependent on the surface texture of the material. Typical values of solar transmittance, at different incident angles, for etched and un-etched glass are shown in Table 1 [12].

Floating photovoltaic system installations tend to adopt a different approach when designing the tilt angles of the installed modules. In the case of such installations, one must consider a tilt angle adequate for the environment in which it will be installed. Tilt angles for floating installations are governed by other facts than optimal power generation, including esthetic impact, wind loading and available space. Researchers from the National Institute of Advanced Industrial Science and Technology installed floating photovoltaic modules at a tilt of 1.3 ° facing south [18,19]. A system near Alicante, Spain [20] was installed with a tilt of 10 ° while the Solarolo project consisted of modules tilted at 8° in order to reduce the footprint of the array and thus, increase the power density output [19]. The Lake Colignola's installation included horizontally mounted PVs with reflectors tilted at −60 ° and 60 ° positioned at the north and south of the modules respectively [21,19].

3. Methodology

3.1. Research description

Non-tracking PV systems have a fixed tilt and orientation optimised for the location in which they are installed. However, offshore photovoltaics will not always stay in the designed tilt and orientation due to the response of the floating structure to incoming waves. Fig. 1 shows the effect that the response of a floating structure to incoming waves can have on the actual tilt of a PV module.

Hence, the effect of motion on offshore PV modules due to incoming waves was studied parametrically and is presented in this paper. The motion of PV modules was divided into three degrees of freedom namely pitch, yaw and roll movements, as shown in Fig. 2. These three movements were chosen in order to cover all the possible degrees of freedom of a moving offshore photovoltaic panel. Any change in Yaw, Pitch and Roll movements were translated into additions to the fixed azimuth and tilt angles chosen for the photovoltaic installation. The effect of each movement on the insolation on offshore PV modules was studied both in simulation and in practice.

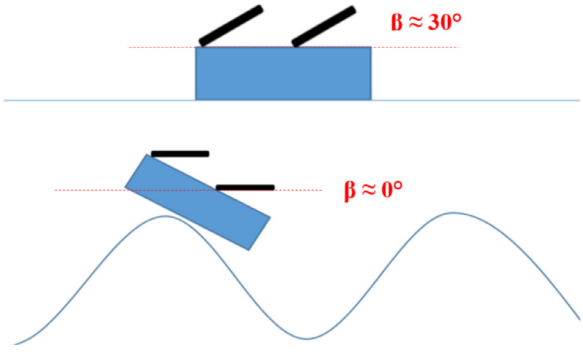

Fig. 1. Floating platform at steady state (TOP) and Floating platform responding to incoming wave (BOTTOM).

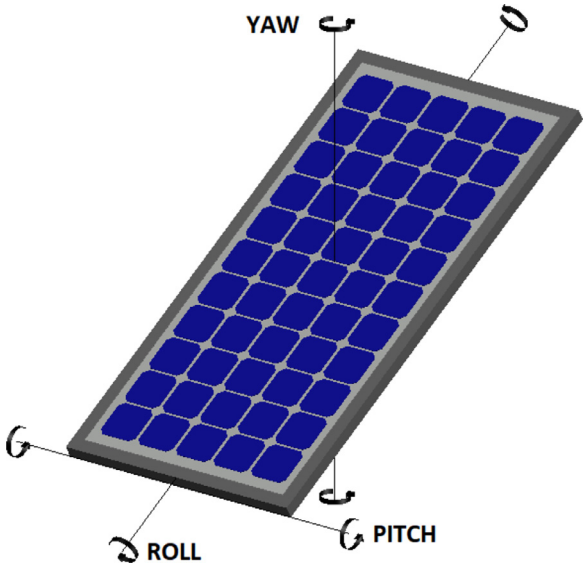

Fig. 2. Pitch, yaw and roll movements on a PV panel.

3.2. Position of the sun

In order to predict the irradiance on a plane at any time during the year one must know the position of the sun relative to a point on earth at that given time. The earth follows an elliptical orbit around the sun. This means that the distance between the sun and the earth, r, is not a constant during the year and is denoted by Eq. (2) [22].

$$r = r_o\left[1 + 0.017\sin\frac{360(N-93)}{365}\right] \tag{2}$$

N is referred to as a Julian day, which is the day number starting from January 1st and r_o accounts for the deviation of the earth's orbit from a circular path. This deviation is usually adequately expressed by a mean value of 1.496×10^8 km [22].

The position of the sun as seen by an observer on Earth usually does not coincide with the local standard time (LST). Hence, in solar calculations, the Apparent Solar Time (AST) is used instead. The difference in minutes between the Apparent Solar Time and the Local Standard Time is given by Eq. (3) [12].

$$AST - LST = 4\left(L_{ST} - L_{LOC}\right) + E \tag{3}$$

Where L_{ST} is the standard meridian for the local time zone and L_{LOC} is the longitude of the observer's location. The parameter E is the equation of time given by Eq. (4) where B is given by Eq. (5) [12].

$$E = 229.2(0.000075 + 0.001868\cos B - 0.032077\sin B - 0.014615\cos 2B - 0.04089\sin 2B) \tag{4}$$

$$B = (N-1)\frac{360}{365} \tag{5}$$

3.3. Total radiation on tilted surfaces

The total radiation on a tilted surface can be divided into two main components, namely Direct (Beam) Radiation $B(\beta,\gamma)$ and Diffused Radiation $D(\beta,\gamma)$. Diffused radiation is further divided in two main components namely diffused radiation originating from the sky $D_a(\beta,\gamma)$, for example due to reflections of clouds, and diffused radiation originating from the ground $D_g(\beta,\gamma)$, example reflections from ground material and buildings. The total radiation on a tilted surface $G(\beta,\gamma)$ is given by Eq. (6).

$$G(\beta,\gamma) = B(\beta,\gamma) + Da(\beta,\gamma) + Dg(\beta,\gamma) \tag{6}$$

Eqs. (7) and (8) relate the angle of incidence of beam radiation on a surface to other known angles.

$$\cos\theta = \sin\delta\sin\emptyset\cos\beta - \sin\delta\cos\emptyset\sin\beta\cos\gamma + \cos\delta\cos\emptyset\cos\beta\cos\omega + \cos\delta\sin\emptyset\sin\beta\cos\gamma\cos\omega + \cos\delta\sin\beta\sin\gamma\sin\omega \quad (7)$$

$$\cos\theta = \cos\theta_z\cos\beta + \sin\theta_z\sin\beta\cos\left(\gamma_s - \gamma\right) \quad (8)$$

Where $\emptyset$ the latitude of the tilted surface, γ is the azimuth of the tilted surface and ω is the hour angle. Various sky models are available in order to predict the total incident radiation on a tilted surface. These can be divided in two main categories, namely the isotropic models and the anisotropic models. The differences between these two model categories lies in the way they look at diffuse radiation. Diffuse radiation can be divided into three parts namely isotropic radiation received uniformly from the entire sky dome, circumsolar diffuse which results from forward scattering in the part of the sky closest to the sun and horizon brightening which is concentrated near the horizon. The latter has more effect in days with clear skies [12].

3.3.1. Isotropic model

The isotropic model is the simplest model to predict the total radiation on an inclined surface. The basic form of this model assumes an isotropic combination of diffuse radiation from the sky and ground-reflected radiation. This means that diffused radiation on a tilted surface is always the same regardless of orientation. An improved version of this model is the isotropic diffuse model by Liu and Jordan [23,12] which considers both isotopic sky diffused radiation, $D_a(\beta,\gamma)$, and diffuse radiation reflected from the ground, $D_g(\beta,\gamma)$. This model gives the total solar radiation on a tilted surface using Eq. (9)[12].

$$G(\beta,\gamma) = B(0,0)R_{T-H} + D_a(\beta,\gamma) + D_g(\beta,\gamma) \quad (9)$$

Where: $D_a(\beta,\gamma) = D(0,0)(\frac{1+\cos\beta}{2})$And: $D_g(\beta,\gamma) = G(0,0)\times\rho_g\times(\frac{1-\cos\beta}{2})$

3.3.2. Anisotropic model

Anisotropic models provide a more accurate calculation of the global radiation on a tilted surface. Hay and Davies factor in the circumsolar diffuse radiation and consider it incident from the same direction as the beam radiation. The Perez Model [24,25] calculates in detail all the three components of diffuse radiation and thus also includes horizon brightening. The diffused radiation on a tilted surface according to the Perez Model is given by Eq. (10) [12]

$$D(\beta,\gamma) = D(0,0)\left[\left(1-F_1\right)\left(\frac{1+\cos\beta}{2}\right) + F_1\frac{a}{b} + F_2\sin\beta\right] \quad (10)$$

and $a = max(0,\cos\theta)$, $b = max(0,\cos\theta_z)$where F_1 and F_2 are circumsolar and horizon brightness coefficients. These coefficients are functions of the zenith angle θ_z, a clearness coefficient ε and a brightness coefficient Δ. F_1 and F_2 are functions of statistically derived coefficients and they are calculated by Eqs. (11) and (12) respectively.

$$F_1 = max\left[0,(f_{11} + f_{12}\Delta + \frac{\pi\theta_z}{180}f_{13}\right] \quad (11)$$

$$F_2 = f_{21} + f_{22}\Delta + \frac{\pi\theta_z}{180}f_{23} \quad (12)$$

Values for the coefficients mentioned in Eqs. (11) and (12) are taken from Table 2, according to the value of the clearness coefficient.

Therefore the complete equation derived from Perez Model representing the irradiance on a tilted plane is given by Eq. (13) [12].

$$G(\beta,\gamma) = B(0,0)\frac{\cos\theta}{\cos\theta_z} + D(0,0)\left[\left(\left(1-F_1\right)\left(\frac{1+\cos\beta}{2}\right) + F_1\frac{a}{b} + F_2\sin\beta\right)\right] + G(0,0)\rho\left(\frac{1-\cos\beta}{2}\right) \quad (13)$$

Table 2
Brightness coefficients for perez model [24,12].

Range of ε	f_{11}	f_{12}	f_{13}	f_{21}	f_{22}	f_{23}
1.000–1.065	−0.008	0.588	−0.062	−0.060	0.072	−0.022
1.065–1.230	0.130	0.683	−0.151	−0.019	0.066	−0.029
1.230–1.5	0.330	0.487	−0.221	0.055	−0.064	−0.026
1.5–1.950	0.568	0.187	−0.295	0.109	−0.152	0.014
1.950–2.800	0.873	−0.392	−0.362	0.226	−0.462	0.001
2.800–4.500	1.132	−1.237	−0.412	0.288	−0.823	0.056
4.500–6.200	1.060	−1.600	−0.359	0.264	−1.127	0.131
6.200-∞	0.678	−0.327	−0.250	0.156	−1.377	0.251

Table 3
Comparison of simulation to practical data for isotropic and perez models.

Type of Sky	Average Deviation from Real Data (Perez Model) (%)	Average Deviation from Real Data (Isotropic Model) (%)
Clear	2.34	6.93
Cloudy	2.02	6.74
Overcast	4.62	9.90

3.4. Simulation

Firstly, a simulation file was created in order to compare the performance of Isotropic and Anisotropic (Perez) models in predicting irradiance on a tilted surface from data of irradiance on a horizontal surface obtained from a weather station installed at the Institute for Sustainable Energy in Marsaxlokk, Malta.

A model from the United States National Oceanic and Atmospheric Administration (NOAA) [26] was used to accurately find the position of the sun on particular dates and at given times. This acquired position was then applied to both Isotropic and Anisotropic (Perez) models in order to derive the total irradiance on a tilted plane. Simulations were carried out for a surface facing South at an inclination of 33 ° (G(33,0)) and compared to real data for three types of sky, namely, clear (Fig. 3), cloudy (Fig. 4) and overcast. Fig. 5 shows the graphical user interface of the simulation file and the result for overcast sky. Real data was obtained from a weather station installed at the Institute for Sustainable Energy in Marsaxlokk, Malta. An albedometer was used to measure the albedo of the weather station area and was found to be 0.35. The deviation of simulation models from real data for the three scenarios are tabulated in Table 3.

As expected from literature [12], the Isotropic Model is the simplest to implement but gives very conservative estimates of global radiation on a tilted surface. Furthermore, the Perez model is more complex to implement but gives results that are more accurate, although slightly overestimated. Hence, the Perez Model was chosen to develop a simulation file in Microsoft Excel in order to predict the loss or gain in yield due to movements in pitch, yaw and roll. Other software would have been easier to implement long simulation algorithms however, Microsoft Excel was chosen in order to provide a tool that can be accessed and edited by the majority of potential users. This simulation focuses on the difference in the irradiance received by a fixed plane and a moving plane due to incoming waves.

The user inputs an equation that characterises the response of the offshore structure to incoming waves in terms of pitch, yaw and roll. Hence, angles are extracted from this equation and added to the fixed azimuth and tilt angles of the installation. Furthermore, weather data is required for that particular day. The essential weather data required by the simulation file are any two of the following:

- Global irradiance on a Horizontal Plane.
- Diffuse radiation on a Horizontal Plane.
- Direct Beam radiation on a Horizontal Plane.

Hence, the file runs two separate algorithms combining a model by the United States National Oceanic and Atmospheric Administration

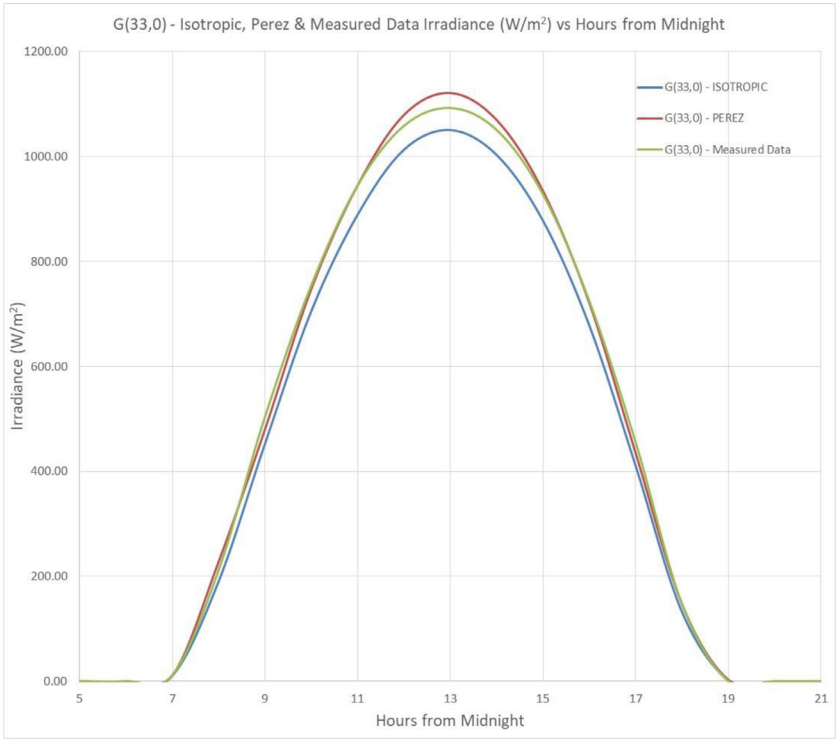

Fig. 3. Clear sky simulation.

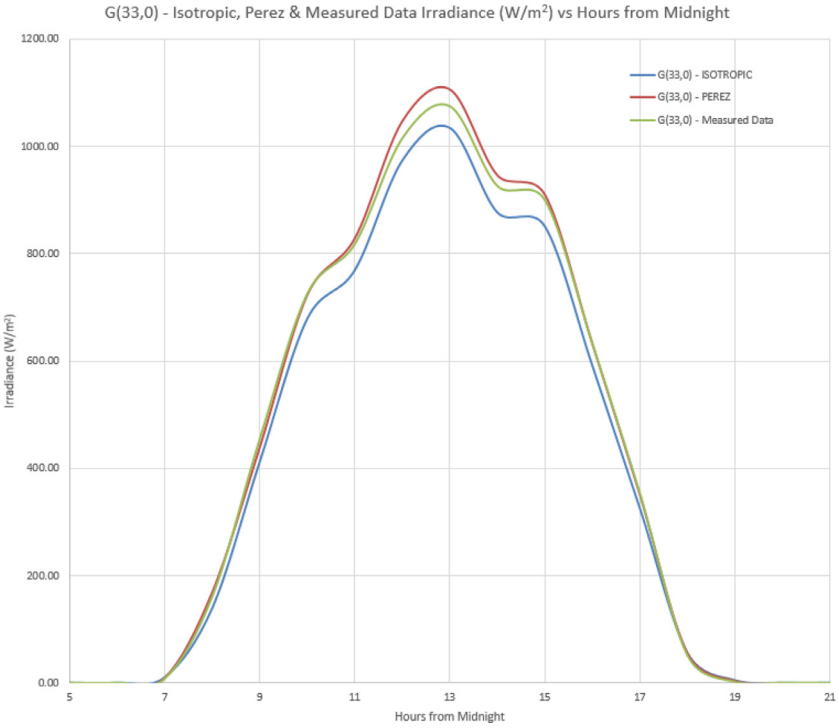

Fig. 4. Cloudy sky simulation.

(NOAA) [26] to find an accurate position of the sun and Perez model to find the global irradiance on a tilted plane. One algorithm derives the global irradiance on a plane with a fixed tilt and orientation while the other algorithm varies the tilt and orientation based on the response equation inputted by the user. Finally, both results of global irradiance are compared together. A parametric simulation was performed comparing a fixed installation on land with an offshore installation installed on a floating structure moving as a response to incoming waves. A pure sinusoidal wave was assumed for all movements. The parameters used for the simulation are shown in Table 4. Hence, another simulation was performed using a movement amplitude of 20 ° and taking a day from each month of the year. The days chosen were close to the 21st of each month in order to include equinoxes and solstices. However, care was taken to choose days with the same sky clarity.

Fig. 5. Comparison file user interface and overcast sky simulation result.

Table 4
Parameters used for irradiance comparison simulation.

Fixed Tilt Angle (β)	Fixed Azimuth Angle (γ)	Movement and Amplitude			
30 °	0 °	Pitch 5 ° Yaw 5 ° Roll 5 °	Pitch 10 ° Yaw 10 ° Roll 10 °	Pitch 15 ° Yaw 15 ° Roll 15 °	Pitch 20 ° Yaw 20 ° Roll 20 °
5 °	0 °	Pitch 5 ° Yaw 5 ° Roll 5 °	Pitch 10 ° Yaw 10 ° Roll 10 °	Pitch 15 ° Yaw 15 ° Roll 15 °	Pitch 20 ° Yaw 20 ° Roll 20 °

Fig. 6. Effect of waves on irradiance: experimental setup.

3.5. Experimental setup

The experimental setup, shown in Fig. 6, was designed in order to verify simulation results in a practical scenario. Poly (methyl methacrylate) material was used to construct two lightweight bases rotating on two axis, similar to the construction of a two-axis solar tracker.

Matrix Solar Sol-A-Meter MK 1-G Pyranometers were attached to these bases in order to obtain irradiance data. These are silicon pyranometers with a spectral response from 0.35 to 1.15 μm with peak sensitivity at 0.85 μm. Their accuracy is ± 5% with a full scale response time of less than 1 ms [27]. High torque servomotors were used in order to achieve the desired movement. Hence, an Arduino UNO board utilizing an ATMEGA328 microcontroller was programmed in order to be able to control the servomotors. The program asks the user to enter the desired Amplitude and period and then outputs a sinusoidal wave using the inputted parameters. This sinusoidal signal is transferred to the servomotors and the desired movements are achieved. Finally, a DATAQ DI-808 data-logger was connected to the pyranometers and a sampling rate of 10 Hz was set in order to accurately acquire all the data points required to represent the response signal. Data was acquired with six decimal places and an accuracy of ± 0.05% of full range. The servomotors were able to perform movements of 1 ° and, due to the high sampling rate, irradiance data was continuously acquired for all different positions. Furthermore, it was ensured that the change in position of the servo motor was slower than the pyranometers response time in order to ensure the correct acquisition of all data points. Fig. 7 shows a data sample representing the effect of pitch movements on the insolation on offshore photovoltaic installations.

Initially a calibration procedure was performed for the two pyranometers in order to get the same irradiance output for the same conditions. It was noted that the available pyranometers' outputs varied slightly from each other and the variation was not constant during the day. This small difference is due to instrument errors reflected in the ± 5% accuracy rating and different deviations from factory calibration over time. While this small difference will have no effect in the normal operation of the pyranometers, it would have an effect on the results of this experiment since the margin of error needs to be minimal. The percentage difference between the moving and the fixed pyranometers was

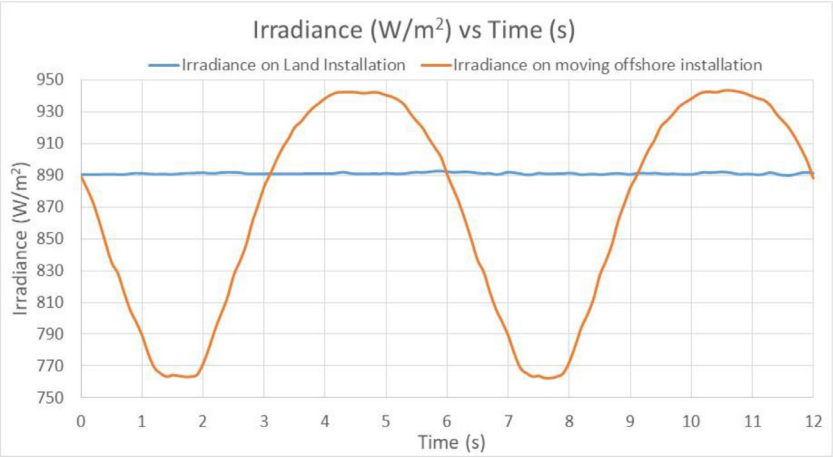

Fig. 7. Data sample showing the effect of pitch movements.

Table 5
Statistical comparison between simulation and experimental data.

$\beta = 30^\circ$ $\alpha = 0^\circ$	Insolation deviation of Offshore from Land (Simulation)			Insolation deviation of Offshore from Land (Experimental)				Average Error between Simulation and Experiment (%)
Movement	Minimum (%)	Maximum	Average (%)	Minimum (%)	Maximum (%)	Average (%)	Average Standard Deviation	
Pitch 20 °	−2.418	−2.550%	−2.484	−2.428	−2.655%	−2.470	0.02165	0.037
Pitch 15 °	−1.365	−1.439%	−1.402	−1.351	−1.430%	−1.381	0.00947	0.008
Pitch 10 °	−0.608	−0.641%	−0.625	−0.589	−0.640%	−0.605	0.01375	0.012
Pitch 5 °	−0.152	−0.161%	−0.156	−0.123	−0.162%	−0.145	0.01282	0.009
Yaw 20 °	−0.131	−0.329%	−0.257	−0.131	−0.346%	−0.262	0.01057	0.026
Yaw 15 °	−0.074	−0.186%	−0.145	−0.072	−0.192%	−0.139	0.01527	0.014
Yaw 10 °	−0.033	−0.083%	−0.065	−0.033	−0.083	−0.065	0.00711	0.006
Yaw 5 °	−0.008	−0.021%	−0.016	−0.008	−0.021%	−0.017	0.01307	0.002
Roll 20 °	−1.800	−1.848%	−1.83	−1.802	−1.850%	−1.83	0.00600	0.009
Roll 15 °	−1.005	−1.041	−1.03	−1.003	−1.227%	−1.09	0.00867	0.053
Roll 10 °	−0.458	−0.472%	−0.47	−0.451	−0.471%	−0.46	0.00965	0.007
Roll 5°	−0.072	−0.129%	−0.10	−0.074	−0.127%	−0.10	0.01038	0.004

expected to be very small from simulation and therefore accuracy was essential. Hence, a calibration procedure was performed immediately before taking readings for each hour. This allowed both pyranometers to start giving the exact same reading before the experimental procedure, described in the flowchart in Fig. 8, was adopted hourly. Pitch and Yaw movements for a tilted surface could be performed directly with the designed setup. However, a slight modification was required in order to perform roll movements for a tilted surface, where an extra piece of wood was added on top of the setup to create the initial tilt of the pyranometers. Finally, data was analyzed and compared to simulation.

4. Results and discussion

4.1. Verification of simulation data

The percentage insolation deviation of an offshore photovoltaic installation from a fixed installation on land due to Pitch, Yaw and Roll movements can be seen in Fig. 9, Fig. 10 and Fig. 11 respectively. These results were obtained in June 2019 for an installation designed with a fixed tilt of 30° and a fixed orientation of 0 ° On one hand, Table 5 shows the maximum and minimum insolation deviation of offshore installations from fixed installations on land, from data obtained from both simulation and experimental setups. On the other hand, Table 5 also shows the average errors between simulation and experimental results. From these results, it can be seen that the largest yield loss is obtained with pitch movements since these movements directly affect the actual installation tilt of the PV modules.

4.2. Simulation of low installation angle

Parametric simulations were performed in order to analyze the effect of wave response motion on the insolation on offshore photovoltaics installed with a designed fixed tilt of 5° This simulation is of interest since a low angle might be the way forward for offshore photovoltaics since this reduces the effects of wind on the installation and allows more PV modules to be installed on each floating structure. Figs. 12, 13 and 14 show the effects of Pitch, Yaw and Roll movements respectively. Additionally, Table 6 presents a statistical representation of these effects.

4.3. Yearly simulations

Parametric simulations were also performed to analyze the effect of Pitch, Yaw and Roll movements on the insolation on offshore photovoltaics throughout all the months of the year. Sinusoidal responses with an amplitude of 20 ° were chosen for these simulations. In order to perform these simulations, weather data for 2019 was taken for days close to the 21st of each month in order to include the major solar events

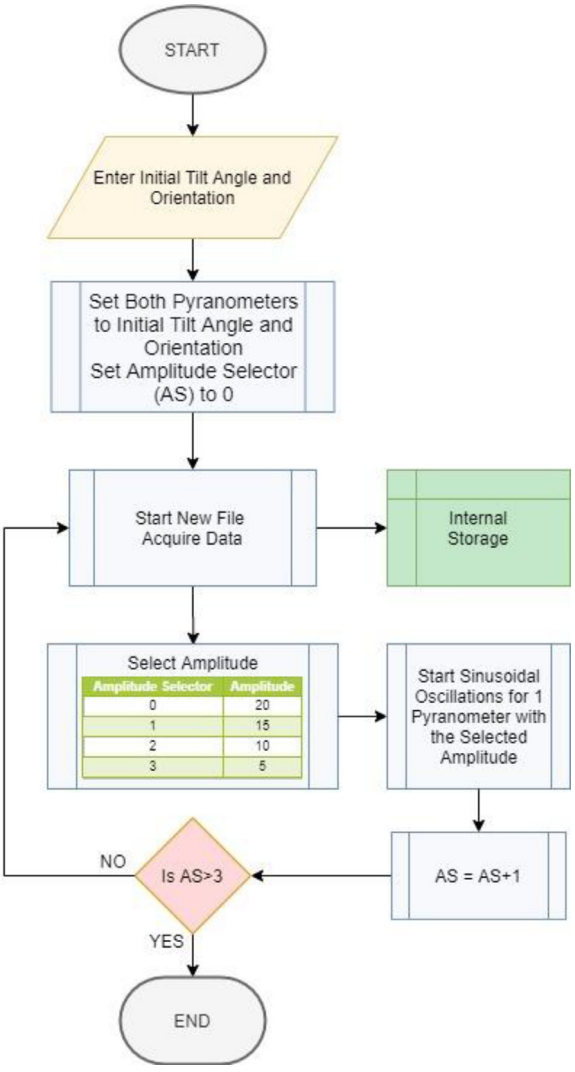

Fig. 8. Floating structure experiment flow chart.

Table 6
Statistical analysis of simulation data for the insolation deviation of an offshore installation from land for a designed fixed tilt of 5 ° and orientation of 0 °

$\beta = 5$ ° $\alpha = 0$ °	Insolation deviation of Offshore from Land (Simulation)		
Movement	**Minimum (%)**	**Maximum (%)**	**Average (%)**
Pitch 20°	−2.409	−2.594	−2.532
Pitch 15°	−1.360	−1.464	−1.429
Pitch 10°	−0.606	−0.652	−0.637
Pitch 5°	−0.152	−0.163	−0.159
Yaw 20°	+0.016 / −0.019	+0.089 / −0.055	−0.022
Yaw 15°	+0.009 / −0.011	+0.050 / −0.031	−0.013
Yaw 10°	+0.004 / −0.005	+0.022 / −0.014	−0.006
Yaw 5°	+0.001 / −0.001	+0.006 / −0.003	−0.00
Roll 20°	−1.881	−2.020	−1.95
Roll 15°	−1.039	−1.186	−1.10
Roll 10°	−0.448	−0.583	−0.48
Roll 5°	−0.051	−0.231	−0.12

namely equinoxes and solstices. However, another criterion that was imposed on the choice of day was that the sky clearness had to be similar in order to be able to do a comparison between different times of the year. Figs. 15 and 16 show the results of these simulations for fixed tilts of 5 ° and 30 ° respectively.

4.4. Discussion

The parametric simulations carried out used the same albedo value for both offshore and land installations. This was decided because the offshore installations we are envisioning will most probably require large floating rafts rather than installing PVs close to the sea surface, as is usually done in floating photovoltaic (FPV) installations. However, in the tool created, albedo can be varied for both offshore and land installations once such data is available. The results presented were simulated based on weather data for the year 2019.

From the yearly simulations, one can note that Yaw movements in December have a much higher negative effect on the insolation than the same movements in May. This is because the irradiance on a tilted plane follows a cosine function. Therefore, although the change in incidence angle is actually lower in January than in June, the change in cos (Θ_i)

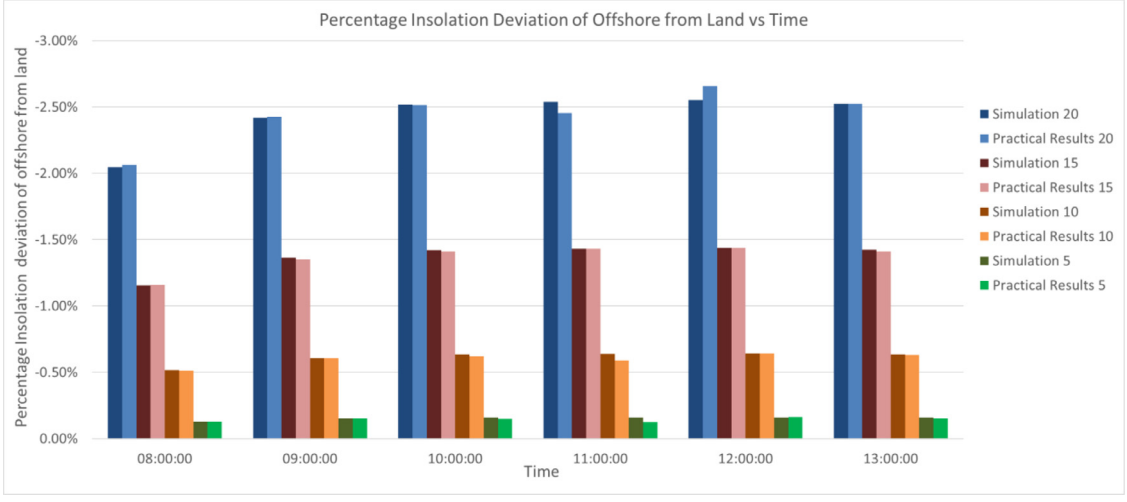

Fig. 9. Comparison between simulation and experimental data: percentage insolation deviation of offshore from land due to pitch movements (03/06/2019, $\beta = 30$ °, $\alpha = 0$ °).

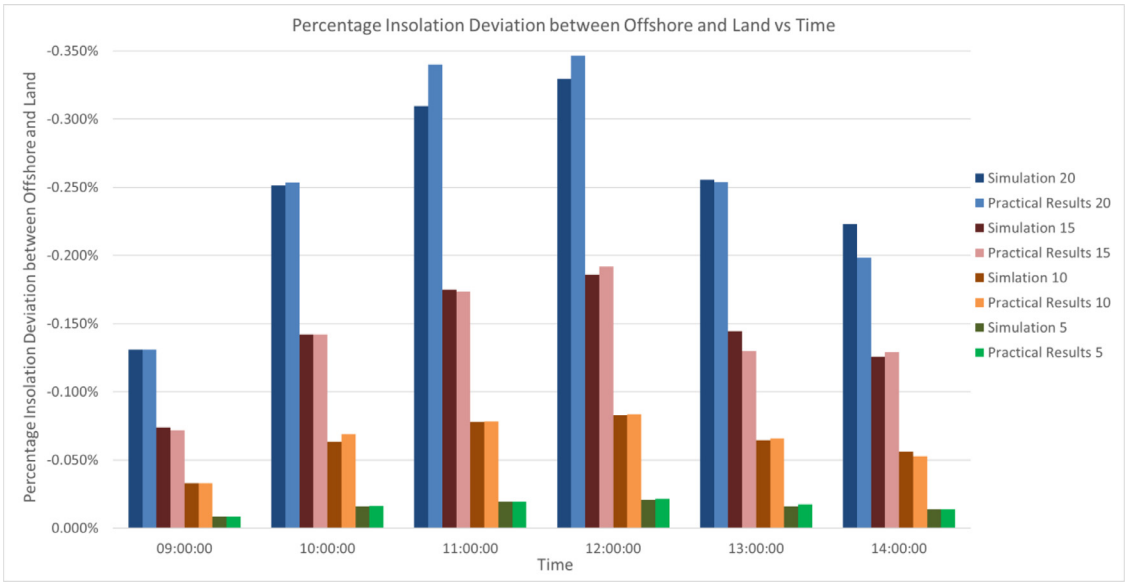

Fig. 10. Comparison between simulation and experimental data: percentage insolation deviation of offshore from land due to yaw movements (06/06/2019, $\beta = 30$ °, $\alpha = 0$ °).

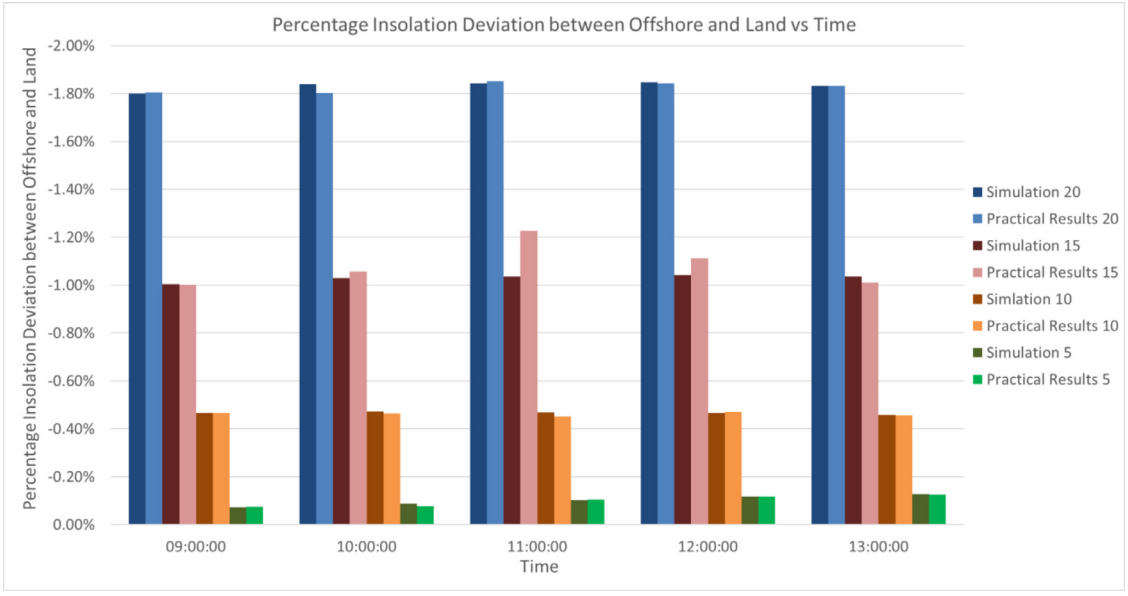

Fig. 11. Comparison between simulation and experimental data: percentage insolation deviation of offshore from land due to roll movements (11/06/2019, $\beta = 30$ °, $\alpha = 0$ °).

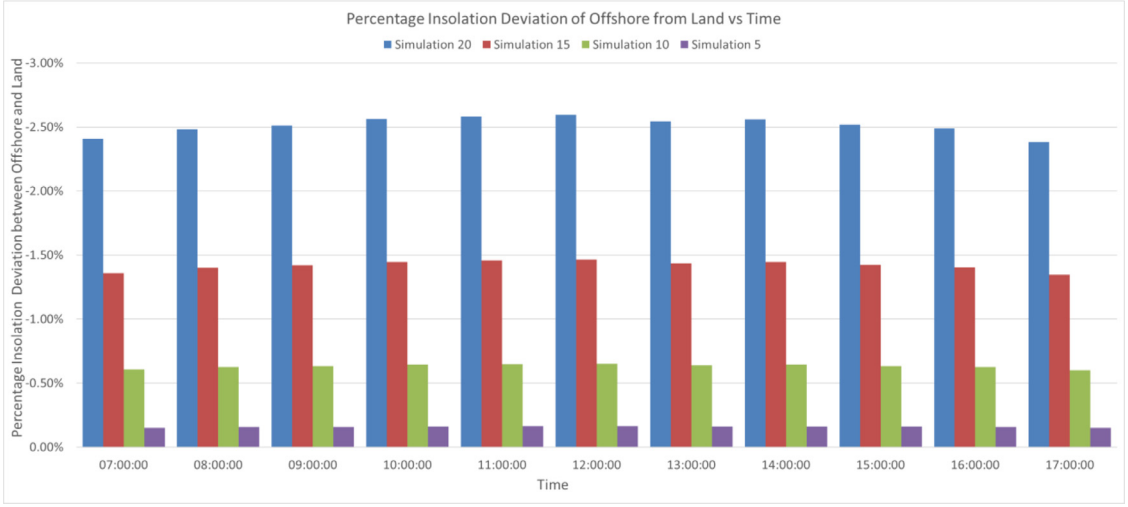

Fig. 12. Percentage insolation deviation of offshore from land due to pitch movements (05/06/2019, $\beta = 5$ °, Fixed $\alpha = 0$ °).

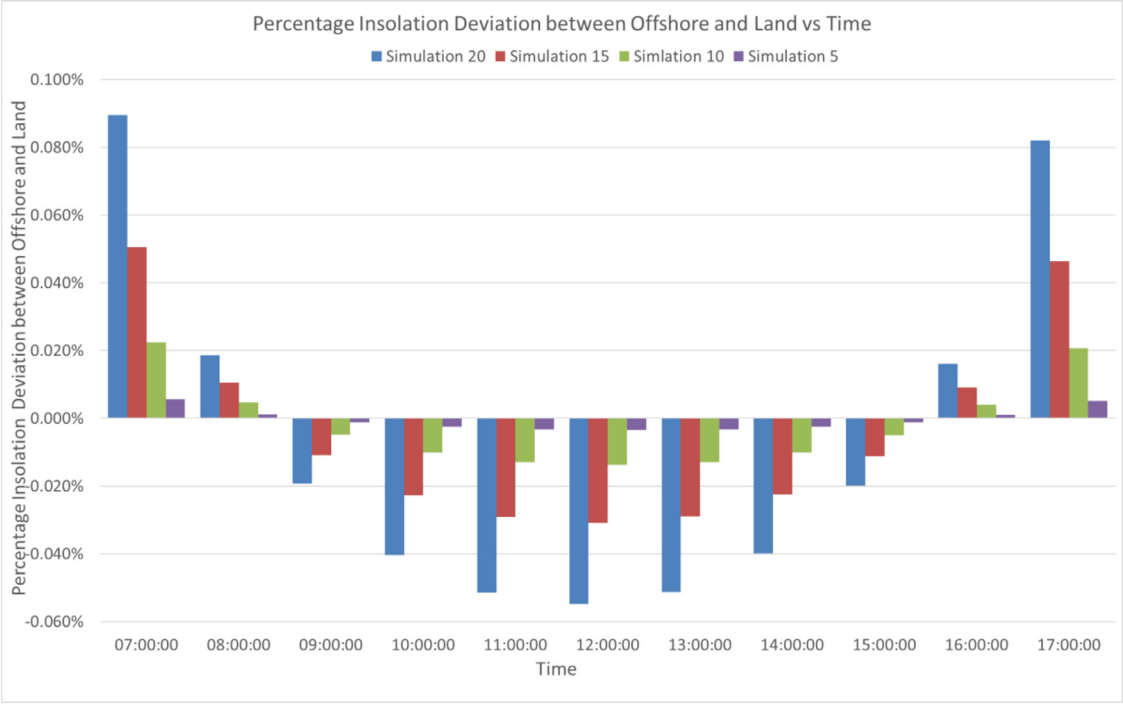

Fig. 13. Percentage insolation deviation of offshore from land due to yaw movements (10/06/2019, $\beta = 5$ °, Fixed $\alpha = 0$ °).

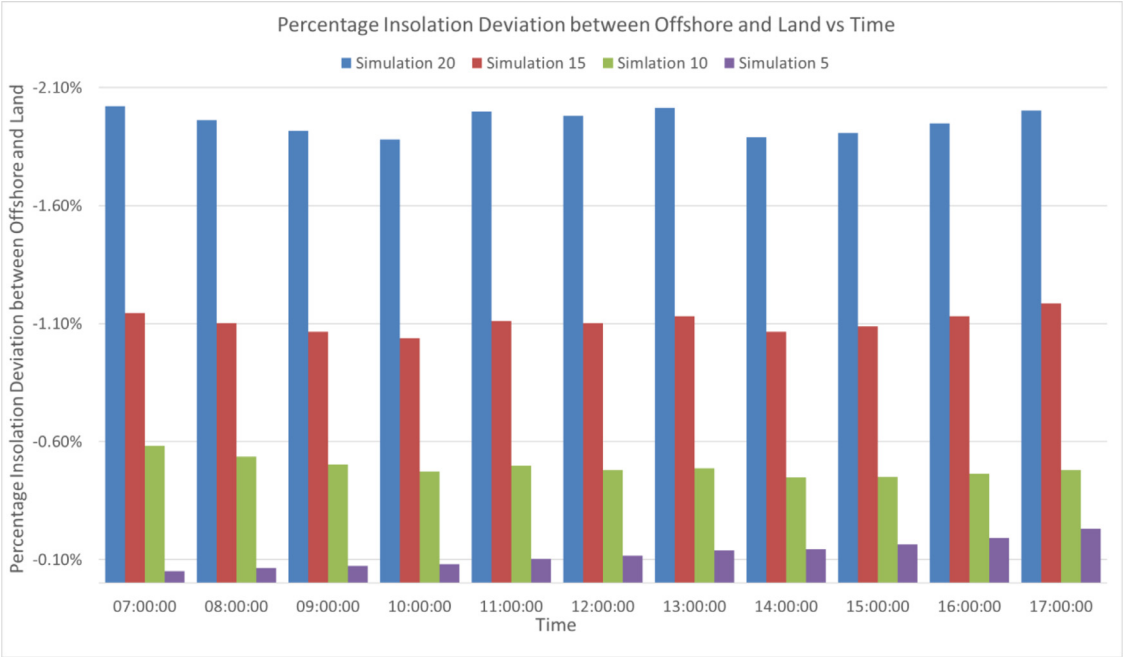

Fig. 14. Percentage insolation deviation of offshore from land due to roll movements (13/06/2019, $\beta = 5$ °, Fixed $\alpha = 0$ °).

is higher. Yaw movements had the highest negative effect of −1.41% in December while a positive effect of up to 0.26% was observed in May.

It can be noted from Figs. 15 and 16 that pitch movements have the highest effect on the insolation. This is because pitch movements directly affect the actual tilt of the installation. Moreover, this effect on an installation with a designed fixed tilt of 30° is more predominant in December than in June. This is because the center of oscillations is closer to the optimal installation tilt angle in June than in December. This is evidenced again in Fig. 15 where, for low tilt angles, seasonal variations in the effect of pitch movements on the insolation are minimal. Pitch movements had the highest negative effect of −2.52% in December and the least negative effect of −1.90% in June. Roll movements had the highest negative effect of −1.41% in May and the least negative effect of −0.65% in October. These movements had a considerable effect on the insolation since they change both the actual tilt and orientation of the PV modules.

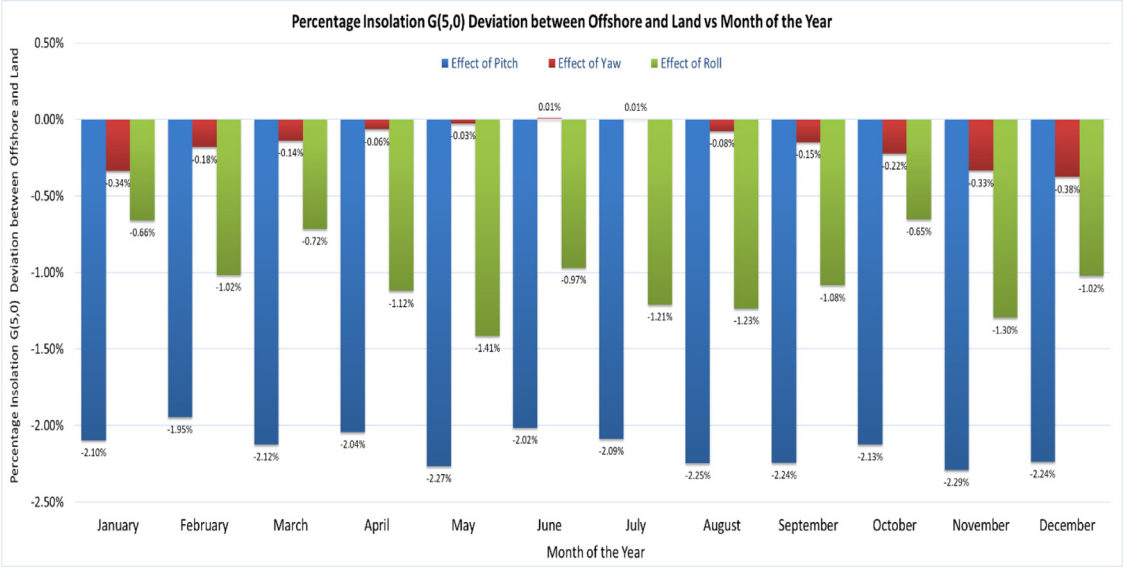

Fig. 15. Percentage insolation deviation between offshore and land throughout the year for a β of 5 ° and α of 0 °

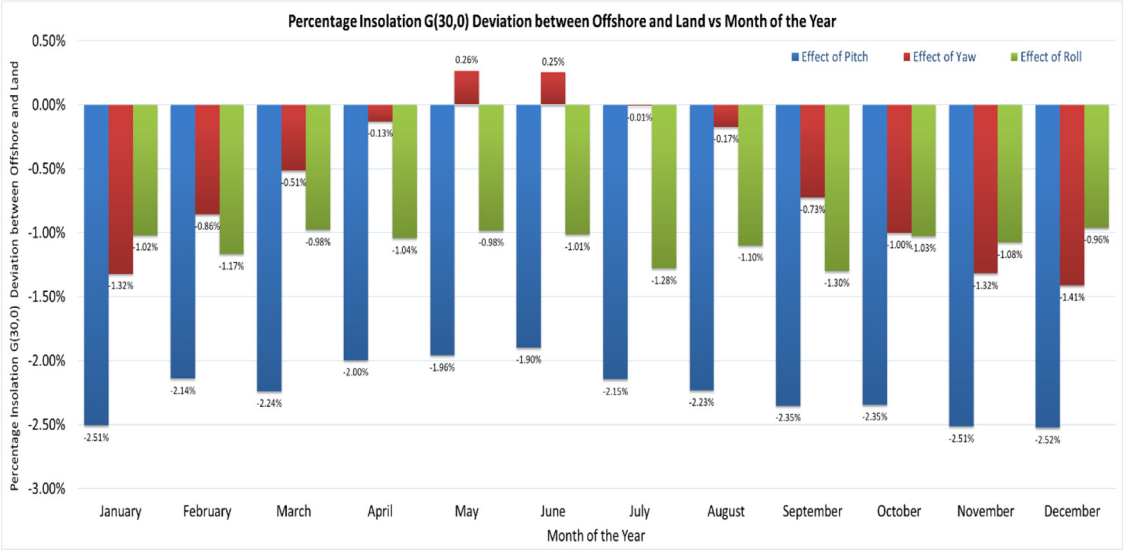

Fig. 16. Percentage insolation deviation between offshore and land throughout the year for a β of 30 ° and α of 0 °

5. Conclusion

Offshore photovoltaic installations have various benefits; however, being a new technological advancement, they also come with a set of unknowns. This study investigated the effect of wave response motion on the insolation on offshore photovoltaic installations. A simulation tool was created in order to allow a system designer to assess the impact that the wave response motion of the floating structure will have on the incident solar energy on the photovoltaic modules. The simulation tool was verified with an experimental setup that simulated sinusoidal wave responses. Finally, a parametric analysis was performed for photovoltaic installations facing south and with fixed tilts of 30° and 5° This parametric analysis was also performed for each month of the year taking days close to the 21st of each month to include the major solar events while still keeping a similar sky clearness. Pitch movements resulted in the most predominant negative effects on the insolation (up to −2.52%) since these movements directly affect the tilt of the installation. Yaw movements had a very small effect on low tilt angle installations (less than −0.38%) since the effect of orientation on such systems is minimal. Finally, this research showed that roll movements could have a considerable effect on the insolation on an offshore photovoltaic installation since these movements change both the actual tilt and orientation of the PV modules.

Declaration of Competing Interest

The authors declare that they have no known competing financial interests or personal relationships that could have appeared to influence the work reported in this paper.

Acknowledgments

We would like to thank Dr. Ing. Charles Yousif for his support in providing some equipment and access to the Institute for Sustainable Energy's weather data.

Funding

This research was supported by the Maltese Regulator for Energy and Water Services (REWS) through the Research Innovation and Development Trust (RIDT) of the University of Malta, as part of the SOLAQUA project.

Data availability

The data and software presented in this study are available on request from the corresponding author.

References

[1] M. Hasanuzzaman, A.B.M.A. Malek, M.M. Islam, A.K. Pandey, N.A. Rahim, Global advancement of cooling technologies for PV systems: a review, Solar Energy 137 (2016) 25–45.
[2] M. MacDonald, "Feasibility study for increasing renewable energy credentials," 2009.
[3] M. Grech, L.M. Stagno, M. Aquilina, M. Cadamuro, and U. Witzke, "Floating photovoltaic installations in Maltese Sea waters," 2016.
[4] A. Sahu, N. Yadav, K. Sudhakar, Floating photovoltaic power plant: a review, Renew. Sustain. Energy Rev. 66 (2016) 815–824.
[5] M. Djordjevic, "40 MW floating PV plant in China connected with Sungrow's inverters," 2017.
[6] P.V. Tech, "Masdar and Indonesian power giant to build world's largest floating solar plant." [Online]. Available: https://www.pv-tech.org/news/masdar-and-indonesian-power-giant-to-build-worlds-largest-floating-solar-pl. [Accessed: 21-Jul-2020].
[7] K. Trapani, D.L. Millar, Proposing offshore photovoltaic (PV) technology to the energy mix of the Maltese islands, Energy Convers. Manag. 67 (2013) 18–26.
[8] L.M. Stagno, "Sustainable energy 2014 : the ise annual conference," in Floating photovoltaics – technological issues, cost and practical implications., 2014, no. March.
[9] Y. Sahu, P. Agrawal, M.D. Shahabuddin, Floating solar photovoltaic system: an emerging technology, in: Proceedings of the National Seminar on Prospects and Challenges of Electrical Power Industry in India - NSPCEPII, 2015, pp. 219–226.
[10] K. Trapani, D.L. Millar, H.C.M. Smith, Novel offshore application of photovoltaics in comparison to conventional marine renewable energy technologies, Renew. Energy 50 (2013) 879–888.
[11] T. Cai, S. Duan, C. Chen, Forecasting power output for grid-connected photovoltaic power system without using solar radiation measurement, in: Proceedings of the 2nd International Symposium on Power Electronics for Distributed Generation Systems, PEDG 2010, 2010.
[12] J.A. Duffie, W.A. Beckman, Solar engineering of thermal processes, 4th Ed., John Wiley & Sons, Inc., 2013.
[13] J.D. Mondol, Y.G. Yohanis, B. Norton, The impact of array inclination and orientation on the performance of a grid-connected photovoltaic system, Renew. Energy 32 (1) (2007) 118–140.
[14] L.M. Stagno, C. Yousif, and M.G. Rebé, "Optimising photovoltaic power generation and useable area by varying the," no. June, pp. 4102–4108, 2013.
[15] S. Beringer, H. Schilke, I. Lohse, G. Seckmeyer, Case study showing that the tilt angle of photovoltaic plants is nearly irrelevant, Sol. Energy (2011).
[16] E.D. Mehleri, P.L. Zervas, H. Sarimveis, J.A. Palyvos, N.C. Markatos, Determination of the optimal tilt angle and orientation for solar photovoltaic arrays, Renew. Energy (2010).
[17] A.B. Rao, G.R. Padmanabhan, Effect of angle of incidence on the performance of a silicon solar cell, Phys. Status Solidi 1 (1) (1970) K29–K32.
[18] Y. Ueda, T. Sakurai, S. Tatebe, A. Itoh, K. Kurokawa, Performance analysis of Pv systems on the water, in: Proceedings of the 23rd European Photovoltaic Solar Energy Conference and Exhibition, 2008.
[19] K. Trapani, M. Red, in: A review of floating photovoltaic installations: 2007-2013, 23, 2015, pp. 524–532.
[20] C. Ferrer-Gisbert, J.J. Ferrán-Gozálvez, M. Redón-Santafé, P. Ferrer-Gisbert, F.J. Sánchez-Romero, J.B. Torregrosa-soler, Torregrosa-soler, "a new photovoltaic floating cover system for water reservoirs, Renew. Energy 60 (2013).
[21] R. Cazzaniga, M. Rosa-Clot, P. Rosa-Clot, G.M. Tina, Floating tracking cooling concentrating (FTCC) systems, in: Proceedings of the Conference Record of the IEEE Photovoltaic Specialists Conference, 2012, pp. 514–519.
[22] A. Luque, S. Hegedus, Handbook of Photovoltaic Science and Engineering, John Wiley & Sons Ltd, England, 2011.
[23] B.Y.H. Liu, R.C. Jordan, The long-term average performance of flat-plate solar-energy collectors, Sol. Energy (1963).
[24] R. Perez, P. Ineichen, R. Seals, J. Michalsky, R. Stewart, Modeling daylight availability and irradiance components from direct and global irradiance, Sol. Energy (1990).
[25] R. Perez, R. Stewart, C. Arbogast, R. Seals, J. Scott, An anisotropic hourly diffuse radiation model for sloping surfaces: description, performance validation, site dependency evaluation, Sol. Energy (1986).
[26] U.S Department of Commerce and NOAA Research, "NOAA earth system research laboratory," 2005. [Online]. Available: https://www.esrl.noaa.gov/gmd/grad/solcalc/calcdetails.html. [Accessed: 08-May-2020].
[27] Matrix Solar Services, "Matrix solar." [Online]. Available: https://www.matrix-solar.com/solar-instruments/.